


Syntheses and characterizations of tetracyanoplatinate(II) complexes with 2-pyridineethanol

Elvan Sayin, Güneş Süheyla Kürkçüoğlu, Okan Zafer Yeşilel & Tuncer Hökelek


To cite this article: Elvan Sayin, Güneş Süheyla Kürkçüoğlu, Okan Zafer Yeşilel & Tuncer Hökelek (2015) Syntheses and characterizations of tetracyanoplatinate(II) complexes with 2-pyridineethanol, Journal of Coordination Chemistry, 68:13, 2271-2285, DOI: 10.1080/00958972.2015.1048239



To link to this article: <http://dx.doi.org/10.1080/00958972.2015.1048239>

 View supplementary material 

 Accepted author version posted online: 05 May 2015.
Published online: 02 Jun 2015.

 Submit your article to this journal 

 Article views: 102

 View related articles 

 View Crossmark data 

Syntheses and characterizations of tetracyanoplatinate(II) complexes with 2-pyridineethanol

ELVAN SAYIN†, GÜNEŞ SÜHEYLÂ KÜRKCÜOĞLU*‡, OKAN ZAFER YEŞİLEL§
and TUNCER HÖKELEK¶

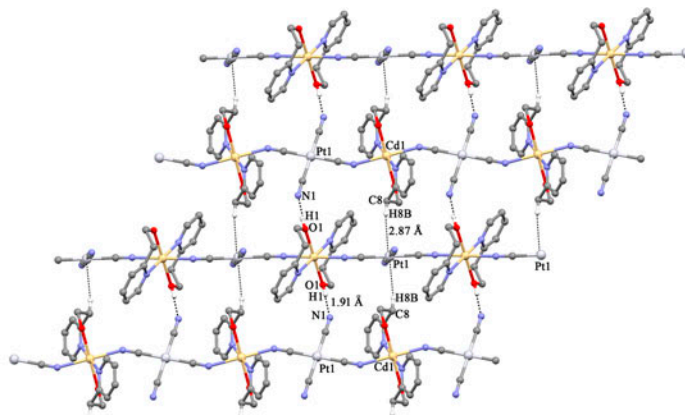
†Graduate School of Natural and Applied Sciences, Physics, Eskişehir Osmangazi University, Eskişehir, Turkey

‡Faculty of Arts and Sciences, Department of Physics, Eskişehir Osmangazi University, Eskişehir, Turkey

§Faculty of Arts and Sciences, Department of Chemistry, Eskişehir Osmangazi University, Eskişehir, Turkey

¶Faculty of Engineering, Department of Physics, Hacettepe University, Ankara, Turkey

(Received 12 November 2014; accepted 21 April 2015)



New cyanide-bridged heteronuclear polymeric complexes, $[\text{Cu}(\text{hepH})_2\text{Pt}(\mu\text{-CN})_2(\text{CN})_2]_n$ (**1**), $[\text{Zn}(\text{hepH})_2\text{Pt}(\mu\text{-CN})_2(\text{CN})_2]_n$ (**2**), and $[\text{Cd}(\text{hepH})_2\text{Pt}(\mu\text{-CN})_2(\text{CN})_2]_n$ (**3**) (2-pyridineethanol abbreviated to hepH), have been synthesized and characterized by elemental analysis, FT-IR and Raman spectroscopies, thermal analysis, and single-crystal X-ray diffraction techniques. Hydrogen bonds play very important roles in the construction of supramolecular structures. From the crystallographic data, it was determined that the crystal packings of **1–3** were composed of rare intermolecular $\text{C-H}\cdots\text{Pt}$ interactions. In addition, these complexes have $\pi\cdots\pi$ and $\text{O-H}\cdots\text{N}$ interactions.

The cyanide-bridged heteronuclear polymeric complexes, $[\text{M}(\text{hepH})_2\text{Pt}(\mu\text{-CN})_2(\text{CN})_2]_n$ ($\text{M} = \text{Cu}(\text{II})$ (**1**), $\text{Zn}(\text{II})$ (**2**) and $\text{Cd}(\text{II})$ (**3**); hepH = 2-pyridineethanol), have been synthesized and characterized by elemental analysis, FT-IR and Raman spectroscopies, thermal analysis, and single-crystal X-ray diffraction techniques. The crystallographic analyses reveal that **1** and **2** crystallize in the triclinic

*Corresponding author. Email: gkurkcuo@ogu.edu.tr

system, space group $P-1$, while **3** crystallizes in the monoclinic system, space group $P2_1/n$. The structures of **1–3** consist of 1-D linear chains in which the M(II) and Pt(II) ions are linked by cyanide ligands. Each M(II) center exhibits a distorted octahedral coordination environment with four nitrogens from two cyanides and two hepH ligands. The 1-D chains are further linked by C–H \cdots Pt and O–H \cdots N hydrogen bonding interactions to construct 3-D supramolecular structures. Thermal stabilities and decomposition products of the complexes were investigated from 30 to 700 °C in air.

Keywords: Tetracyanoplatinate(II) complex; 2-Pyridineethanol complex; Heteronuclear complex; Cyanide-bridged complex; 1-D complex

1. Introduction

A combination of interesting structural and material properties of cyanide-bridged heteronuclear complexes have made this area heavily explored. Polymeric metal complexes are formed, especially with macromolecules formed by metal–metal or metal–ligand–metal bridge connections in one-, two-, or three-dimensions [1]. For designing coordination polymers of intended dimensionality having a specific property, the proper choice of suitable metal and bridging or chelating ligands is important. Most ligands contain carboxylate, cyanide, or pyridine-type groups [2, 3]. Cyanide, a simple pseudo halide, is widely used to synthesize 1-D, 2-D, or 3-D structures because of the ability to behave as σ -donor and π -acceptor, negative charge, and ambidentate character. Cyanide-bridged transition metal coordination polymers have found several applications [4].

Investigation on cyanide-bridged polymeric metal complexes using tetracyanoplatinate(II) as building blocks are limited [5–10]. Because tetracyanoplatinate(II) can use different numbers of cyanide groups to bind to other metal ions, a range of solid-state structures exist. The formation of the supramolecular assemblies has been rationalized with competition between coordinative forces and hydrogen bonding interactions crucial in the determination of final solid-state packing. The packing of 1-D/2-D coordination polymers in the solid state is generally controlled by weak interactions [11], and these weak forces also play many important roles for 3-D coordination polymers [12]. The weaker non-covalent interactions, such as hydrogen bonding [13], $\pi\cdots\pi$ stacking [14], and C–H \cdots M [15, 16] are important for the overall superstructure obtained [17, 18].

In our previous study, we reported tetracyanonickelate(II) and tetracyanopalladate(II) complexes with hepH [19, 20]. To the best of our knowledge, neither crystallographic nor vibrational analysis study of tetracyanoplatinate(II) with hepH has been reported. As a continuation of our previous studies, three cyanide-bridged heteronuclear polymeric complexes of Cu(II), Zn(II), and Cd(II) with hepH and $[\text{Pt}(\text{CN})_4]^{2-}$ have been synthesized. In the present paper, we describe the syntheses, FT-IR, and Raman spectra, thermal studies [thermogravimetric analysis (TG), derivative thermogravimetric analysis (DTG) and differential thermal analysis (DTA)], and crystal structures of three 1-D heteropolynuclear complexes of Cu(II), Zn(II) and Cd(II) ions with 2-pyridineethanol (hepH) and $[\text{Pt}(\text{CN})_4]^{2-}$.

2. Experimental

2.1. Materials

All materials such as copper(II) chloride dihydrate ($\text{CuCl}_2 \cdot 2\text{H}_2\text{O}$, 99%), zinc(II) chloride (ZnCl_2 , 96%), cadmium(II) chloride hemi(pentahydrate) ($\text{CdCl}_2 \cdot 2.5\text{H}_2\text{O}$, 81%), platinum(II) chloride (PtCl_2 , 99%), potassium cyanide (KCN, 96%), and 2-pyridineethanol ($\text{C}_7\text{H}_9\text{NO}$, 98%) were used as received.

2.2. Syntheses of the complexes

2.2.1. $\text{M}[\text{Pt}(\text{CN})_4] \cdot \text{H}_2\text{O}$ (M = Cu, Zn, and Cd). To water solution of PtCl_2 (0.265 g, 1 mmol) was added a solution of KCN (0.260 g, 4 mmol) in water (10 mL) and colorless $\text{K}_2[\text{Pt}(\text{CN})_4] \cdot \text{H}_2\text{O}$ was crystallized. $\text{K}_2[\text{Pt}(\text{CN})_4] \cdot \text{H}_2\text{O}$ (0.395 g, 1 mmol) to which was added metal chloride solutions ($\text{CuCl}_2 \cdot 2\text{H}_2\text{O} = 0.170$ g, $\text{ZnCl}_2 = 0.136$ g or $\text{CdCl}_2 \cdot 2.5\text{H}_2\text{O} = 0.228$ g, 1 mmol) became $\text{M}[\text{Pt}(\text{CN})_4] \cdot \text{H}_2\text{O}$. The colors of $\text{Cu}[\text{Pt}(\text{CN})_4] \cdot \text{H}_2\text{O}$, $\text{Zn}[\text{Pt}(\text{CN})_4] \cdot \text{H}_2\text{O}$ and $\text{Cd}[\text{Pt}(\text{CN})_4] \cdot \text{H}_2\text{O}$ are green, gray and yellow, respectively.

2.2.2. $[\text{M}(\text{hepH})_2\text{Pt}(\mu\text{-CN})_2(\text{CN})_2]_n$ (M = Cu, Zn, and Cd). A mixture of $\text{Cu}[\text{Pt}(\text{CN})_4] \cdot \text{H}_2\text{O}$ (0.380 g, 1 mmol) in water (10 mL) and hepH (0.246 g, 2 mmol) in ethanol (10 mL) was stirred at 55 °C for 4 h in a temperature-controlled bath. The obtained solution was filtered and kept for crystallization at room temperature. Green $[\text{Cu}(\text{hepH})_2\text{Pt}(\mu\text{-CN})_2(\text{CN})_2]_n$ (**1**) block-shaped single crystals were obtained by slow evaporation after one week. The complex was analyzed for C, H, and N with the following results: Yield: 0.280 g, 45.97% based on $\text{CuCl}_2 \cdot 2\text{H}_2\text{O}$. Anal. Calcd for $\text{C}_{18}\text{H}_{18}\text{N}_6\text{O}_2\text{PtCu}$ (**1**) ($M_w = 609.01$ g mol⁻¹): C, 35.50; H, 2.98; N, 13.80%. Found: C, 34.87; H, 2.73; N, 13.01%.

Complexes **2** and **3** were obtained in a similar method to **1**, but Cu(II) was replaced by Zn (II) (0.382 g) or Cd(II) (0.429 g). Orange and colorless crystals of **2** and **3** were obtained (yield: 0.313 g, 51.31% based on ZnCl_2 for **2** and 0.325 g, 49.46% based on $\text{CdCl}_2 \cdot 2.5\text{H}_2\text{O}$ for **3**). Anal. Calcd for $\text{C}_{18}\text{H}_{18}\text{N}_6\text{O}_2\text{PtZn}$ (**2**) ($M_w = 610.85$ g mol⁻¹): C, 35.39; H, 2.97; N, 13.76%. Found: C, 35.05; H, 3.17; N, 13.80%. Anal. Calcd for $\text{C}_{18}\text{H}_{18}\text{N}_6\text{O}_2\text{PtCd}$ (**3**) ($M_w = 657.87$ g mol⁻¹): C, 32.86; H, 2.76; N, 12.77%. Found: C, 33.45; H, 2.98; N, 13.65%.

2.3. Physical measurements

Elemental analyses (C, H, and N) were carried out by standard methods using a CHNS-932 (LECO) analyzer at the Middle East Technical University Central Laboratory in Ankara, Turkey. FT-IR spectra of hepH and the complexes were carried out at room temperature by a Perkin-Elmer FT-IR 100 spectrometer from 4000 to 250 cm⁻¹. Resolution was set to 4 cm⁻¹; signal/noise ratio was established by 16 scans with attenuated total reflection. Raman spectra of the complexes were recorded from 4000 to 250 cm⁻¹ via a Bruker Senterra Dispersive Raman Microscope using the 785 nm line of a 3B diode laser. The TG, DTA, and DTG measurements were carried out using a Perkin-Elmer Diamond TG/DTA Thermal Analysis instrument under static air at a heating rate of 10 K min⁻¹ from 30 to 700 °C using platinum crucibles.

2.4. Crystallographic analyses

Crystallographic data were recorded on a Bruker Kappa APEXII CCD area-detector diffractometer using Mo K_{α} radiation ($\lambda = 0.71073 \text{ \AA}$) at room temperature. Absorption corrections by multi-scan [21] were applied. Structures were solved by direct methods [22] and refined by full-matrix least squares against F^2 using all data [22]. All non-H atoms were refined anisotropically. In **1**, **2**, and **3**, H1 and H1A (for OH) were located in difference syntheses and refined isotropically. In all compounds, the remaining hydrogens were positioned geometrically at 0.93 \AA (CH) and 0.97 \AA (CH_2) from the parent carbons; a riding model was used during the refinement processes and the $U_{\text{iso}}(\text{H})$ values were constrained to be $1.2U_{\text{eq}}$ (carrier atom).

3. Results and discussion

3.1. Vibrational spectra

FT-IR and Raman spectra of the complexes are illustrated in figures 1 and 2, respectively. The assignments of hepH wavenumbers observed in the FT-IR and Raman spectra of the

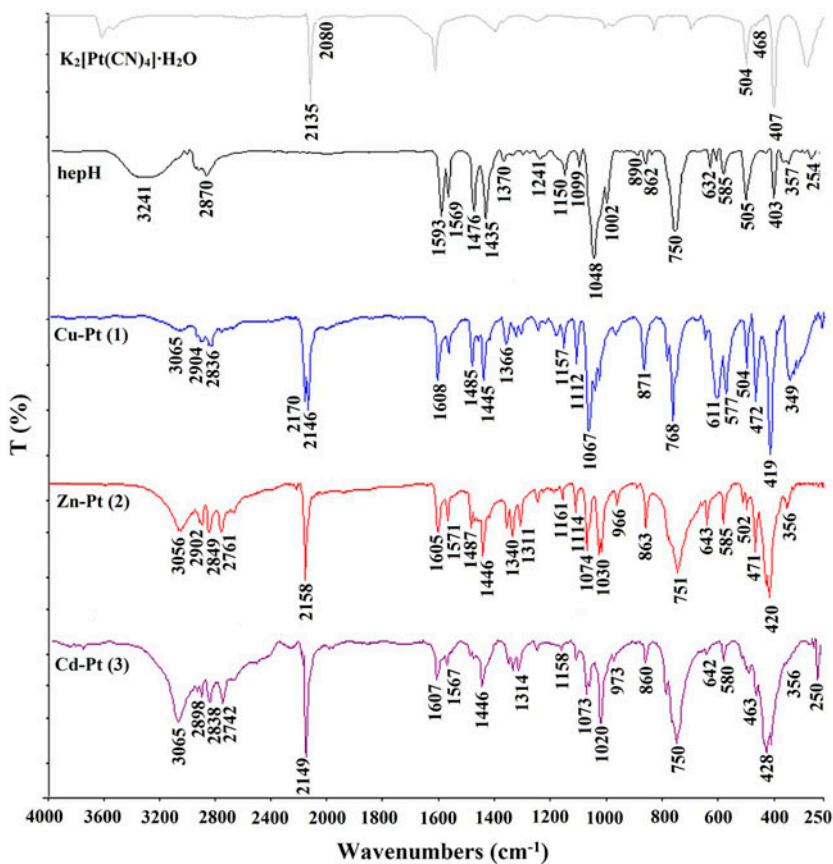


Figure 1. The FT-IR spectra of $\text{K}_2[\text{Pt}(\text{CN})_4] \cdot \text{H}_2\text{O}$, hepH and 1–3.

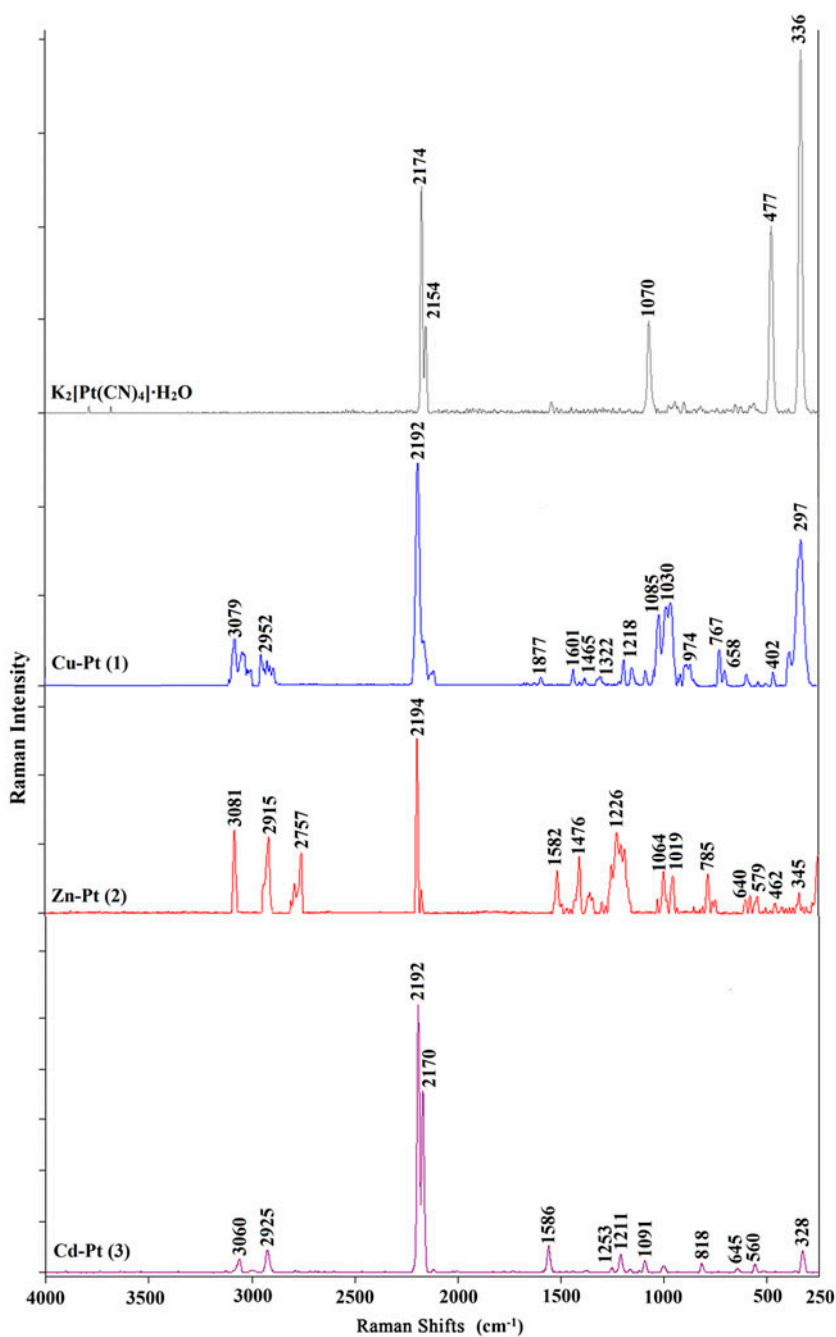


Figure 2. The Raman spectra of $K_2[Pt(CN)_4] \cdot H_2O$ and 1–3.

complexes are given in table 1, together with the wavenumbers for hepH [19]. Considerable shifts to higher or lower wavenumbers occur in the presence of numerous absorption bands in spectra of the complexes due to characteristic OH, CH_2 , CH, and ring vibrations. Infrared

Table 1. The FT-IR and Raman wavenumbers of hepH and the complexes (cm^{-1}).

No.	Assignments (PED%) [19]	hepH											
		Experimental (liquid)						Calculated					
		1		2		3		1		2		3	
FT-IR	Raman	FT-IR	Raman	FT-IR	Raman	FT-IR	Raman	FT-IR	Raman	FT-IR	Raman	FT-IR	Raman
1	$\nu(\text{OH})$ (100)	3382 m	—	3677	3106 sh	—	3108 vw	—	3105 vw	—	—	3105 vw	—
2	$\nu(\text{CH})$ (90)	3087 vw	3075 vw	3066	3070 vw	3080 m	3069 w	3081 m	3065 m	3061 m	—	3065 w	—
3	$\nu(\text{CH})$ (99)	3071 vw	—	3055	3055vw	3045 vw	3056 w	—	—	—	—	3055 w	—
4	$\nu(\text{CH})$ (91)	—	—	3041	—	—	—	—	—	—	—	—	—
5	$\nu(\text{CH})$ (94)	3013 m	3024 vw	3020	2963 w	3003 vw	2963 w	3005 w	2961 vw	3007 m	—	—	—
6	$\nu_{\text{as}}(\text{CH}_2) + \nu_{\text{as}}(\text{CH}_2)$ (99)	2954 m	3008 vw	2971	2942 w	—	2952 w	—	2948 w	—	—	—	—
7	$\nu_{\text{as}}(\text{CH}_2) + \nu_{\text{as}}(\text{CH}_2)$ (87)	2929 m	2925 vw	2951	2917 m	2953 m	2923 w	2962 vw	2931 w	2925 vw	—	—	—
8	$\nu_{\text{as}}(\text{CH}) + \nu_s(\text{CH}_2)$ (93)	2904 vw	—	2911	2904 vw	2923 vw	2902 w	2915 m	2898 w	—	—	—	—
9	$\nu_s(\text{CH}_2) + \nu_s(\text{CH}_2)$ (94)	2870 m	—	2900	2872 w	2862 m	2849 m	2858 w	2842 m	2856 w	—	—	—
10	$\nu_{\text{ring}}(\text{C}-\text{C})$ (54)	1593 s	1582 m	1610	1608 m	1602 m	1605 m	1612 vw	1607 m	1586 m	—	—	—
11	$\nu_{\text{ring}}(\text{C}-\text{C})$ (52)	1569 m	1554 w	1591	1569 m	1573 m	1571 m	1578 vw	1570 m	1560 w	—	—	—
12	$\delta_{\text{ring}}(\text{CH}_2)$ (72)	1506 vw	—	1495	1508 vw	1546 vw	1504 vw	1552 vw	1507 vw	1507 vw	—	—	—
13	$\delta(\text{CH})$ (16) + $\nu(\text{NC})$ (19) + $\delta(\text{HCN})$ (33)	1476 s	1460 sh	1485	1485 m	1481 m	1487 m	1482 vw	1487 m	—	—	—	—
14	$\delta(\text{CH}_2)$ (75)	1435 s	—	1466	1463 w	1466 m	1446 m	1478 w	1475 m	1475 vw	—	—	—
15	$\delta(\text{CCH})$ (51)	1417 sh	—	1446	1445 m	1428 w	1423vw	1434 vw	1446 s	1443 w	—	—	—
16	$\delta(\text{COH})$ (13) + $\delta(\text{CH}_2)$ (19) + $\text{t}(\text{CCCH})$ (41)	1370 m	1392 vs	1392	1366 w	1391 vw	1359 m	1379 w	1352 m	1374 m	—	—	—
17	$\delta(\text{COH})$ (19) + $\delta(\text{CH}_2)$ (34) + $\text{t}(\text{CCCH})$ (10)	1337 sh	1320 sh	1364	1359 w	1357 m	1340 m	1352 w	1336 m	—	—	—	—
18	$\delta(\text{CCH})$ (33) + $\delta(\text{HCN})$ (26)	1316 vw	1295 sh	1325	1310 w	1298 vw	1311 m	1304 w	1314 m	—	—	—	—
19	$\delta(\text{COH})$ (20) + $\text{t}(\text{CCCH})$ (29)	1301 w	—	1304	1285 vw	—	1284 vw	—	1285 sh	—	—	—	—
20	$\nu(\text{NC})$ (29) + $\delta(\text{HCN})$ (12) + $\delta(\text{CCH})$ (15)	1278 sh	—	1289	1277 vw	1273 vw	—	1287 vw	1274 vw	—	—	—	—
21	$\nu(\text{NC})$ (39) + $\text{t}(\text{CCCH})$ (10)	1241 m	1234 m	1263	1249 w	1253 m	1251 w	1252 w	1250 w	1253 w	—	—	—
22	$\delta(\text{CC})$ (24) + $\delta(\text{CCH})$ (12) + $\delta(\text{CNC})$ (10)	1223 w	—	1226	1223 w	1219 m	1228 vw	1226 m	1228 vw	1211 w	—	—	—
23	$\nu(\text{CC})$ (11) + $\delta(\text{CCH})$ (74)	1150 m	1193 vw	1161	1157 w	1192 vw	1161 w	1189 m	1162 w	1163 m	—	—	—
24	$\delta(\text{COH})$ (16) + $\delta(\text{CCH})$ (20)	1099 m	—	1104	1112 s	1159 m	1114 m	1164 m	1109 m	1121 vw	—	—	—
25	$\nu(\text{CC})$ (12) + $\delta(\text{CCH})$ (21)	—	—	1104	1067 m	1086 m	1074 s	1070 m	1073 s	1091 vw	—	—	—
26	$\nu(\text{CC})$ (49)	1048 s	1065 s	1056	1046 s	1030 m	1030 s	1026 m	1024 s	1033 m	—	—	—
27	$\nu(\text{OC})$ (87)	1002 s	1011 s	1038	1030 m	—	1021 m	1019 m	1020 m	1003 w	—	—	—
28	$\nu(\text{CC})$ (49)	993 sh	—	1023	996 w	995 vw	999 w	1000 vw	999 sh	—	—	—	—
29	$\nu(\text{CC})$ (38) + $\delta(\text{HCO})$ (10)	—	—	1004	972 m	—	—	975 w	974 w	—	—	—	—
30	$\text{t}(\text{CCCH})$ (48) + $\text{t}(\text{HCCN})$ (17) + $\text{t}(\text{CCCC})$ (12)	966 vw	971 vw	997	964 m	965 m	966 w	968 w	962 vw	—	—	—	—
31	$\nu(\text{CN})$ (10) + $\nu(\text{CC})$ (11) + $\delta(\text{CCH})$ (25)	952 w	968 vw	996	953 vw	952 vw	953 sh	953 vw	950 vw	—	—	—	—
32	$\text{t}(\text{HCCC})$ (13) + $\text{t}(\text{HCCN})$ (54) + $\text{t}(\text{CCCN})$ (14)	940 sh	925 vw	966	947 sh	944 w	943 vw	931 vw	940 vw	938 w	—	—	—
33	$\text{t}(\text{HCCC})$ (48) + $\text{t}(\text{HCCN})$ (24)	890 m	852 w	894	897 vw	871 vw	893 w	883 vw	893 w	—	—	—	—

34	$\nu(\text{CC})(22) + \delta(\text{NCC})(11) + \delta(\text{CCC})(23)$	862 m	822 vw	844	871 m	858 vw	863 m	857 vw	861 m	—
35	$\tau(\text{HCCC})(47)$	781 sh	793 m	786	787 w	793 vw	784 m	785 m	788 m	786 m
36	$\tau(\text{HCCC})(13) + \tau(\text{HCCN})(30) + \tau(\text{CCCC})(12) + \tau(\text{CCCN})(11) + \tau(\text{CNCC})(19)$	750 vs	765 sh	770	768 s	768 vw	751 s	748 w	751 s	737 vw
37	$\delta(\text{CCO})(17) + \delta(\text{NCC})(32) + \delta(\text{CCN})(17)$	728 sh	645 m	732	694 vw	658 w	697 sh	666 w	695 sh	—
38	$\delta(\text{CCO})(17) + \delta(\text{NCC})(32) + \delta(\text{CNC})(17)$	632 m	623 sh	640	652 w	658 w	643 vw	640 w	642 m	645 w
39	$\delta(\text{CCO})(24) + \delta(\text{CNC})(15)$	585 s	588 m	613	577 m	569 vw	585 m	579 w	581 m	560 vw
40	$\tau(\text{HCCC})(13) + \tau(\text{CNCC})(35)$	505 m	477 vw	510	504 m	501 m	502 w	514 w	518 vw	517 w
41	$\tau(\text{HCCC})(18)$	403 m	417 vw	411	394 w	402 m	390 vw	397 vw	399 sh	—
42	$\delta(\text{CCN})(55)$	357 m	350 sh	364	357 w	343 sh	353 w	349 w	355 w	—
43	$\nu(\text{CC})(15) + \tau(\text{HOCC})(15) + \delta(\text{OCC})(32)$	336 sh	335 vw	344	322 vw	312 m	333 vw	315 vw	337 w	—
44	$\tau(\text{HOCC})(76)$	285 m	283 m	292	288 w	—	289 vw	280 vw	298 vw	—
45	$\delta(\text{CCO})(23) + \tau(\text{CCCC})(14)$	254 m	—	259	262 w	251 m	—	254 vw	259 w	—
46	$\delta_s(\text{CH}_2)$	—	—	—	—	—	—	—	—	—
47	$\delta_s(\text{CH}_2)$	—	—	—	—	—	—	—	—	—
48	$\delta_s(\text{skeletal})$	—	—	—	—	—	—	—	—	—

Notes: ν , stretching; δ , bending; τ , torsion; r, ring; s, strong; m, medium; w, weak; sh, shoulder; v, very. Theoretical frequencies scaled by 0.960 in the high wavenumbers region and by 0.988 in the low wavenumbers region (below 1800 cm^{-1}). Only potential energy distribution values greater than 10% are given.

bands at 3106 (**1**), 3108 (**2**), and 3105 cm^{-1} (**3**) are assigned to the OH stretching modes (not observed in Raman spectra). In the complexes, the CH modes are observed from 3070 to 2961 cm^{-1} (in FT-IR spectra) and 3030–3061 cm^{-1} (in Raman spectra). The CH_2 asymmetric stretches are generally observed at 3000–2900 cm^{-1} , while the CH_2 symmetric stretch will appear between 2900 and 2800 cm^{-1} [23]. In the complexes, CH_2 asymmetric stretching vibrations are observed at 2952–2917 cm^{-1} in FT-IR spectra and 2962–2925 cm^{-1} in Raman spectra. In FT-IR spectra of the complexes, CH_2 symmetric vibrations are observed from 2904 to 2842 cm^{-1} . The ring stretching (ν_{ring}) vibrations are at 1608–1569 cm^{-1} for the complexes. It is clear from table 1 that small shifts toward high and low frequencies in the complexes are caused by coordination. When the aromatic ring nitrogen complexes, certain ring modes, particularly modes of 1600–1400 cm^{-1} , increase due to coupling with M–N (ligand) bond vibrations. Analogous shifts on coordination have been observed in the vibrational spectra of the other metal coordinated pyridine complexes [24, 25]. The C–O stretching modes are at 1030 cm^{-1} (**1**), 1021 cm^{-1} (**2**), and 1020 cm^{-1} (**3**) in the FT-IR spectra. These modes are at 1019 cm^{-1} (**2**) and 1020 cm^{-1} (**3**) in the Raman spectra. The spectral features and assignments of the in-plane and out-of-plane bending vibrations are included in table 1.

The presence of cyanide bridges in the polymeric complexes are shown by the splitting of $\nu(\text{CN})$ which appear at 2200–2000 cm^{-1} for cyanide complexes. The $\nu(\text{CN})$ stretches of the complexes are generally higher than the value for free CN^- . According to this, the assigned wavenumbers and modes for $[\text{Pt}(\text{CN})_4]^{2-}$ in the complexes are given in table 2, together with the wavenumbers of $[\text{Pt}(\text{CN})_4]^{2-}$ [26]. In the FT-IR spectrum of $\text{K}_2[\text{Pt}(\text{CN})_4]\cdot\text{H}_2\text{O}$, it is at 2135 cm^{-1} . Cyanide stretching vibration of ionic cyanides, NaCN and KCN, was observed at 2080 cm^{-1} [27]. This peak shifted to 2150 cm^{-1} in $[\text{Pt}(\text{CN})_4]^{2-}$ as a result of coordination [27]. In the Raman spectra, the cyanide stretching modes are at 2174 and 2154 cm^{-1} for $[\text{Pt}(\text{CN})_4]^{2-}$. Special attention has been paid to the numbers and positions of the $\nu(\text{CN})$ absorption bands in the infrared spectrum, because they may help to reveal the number and the type (terminal or bridging) of cyanide groups [28]. For tetracyanoplatinate(II) complexes, coordination of CN shifts $\nu(\text{CN})$ to higher frequencies and the range for terminal cyanide ligands extend from 2120 to 2140 cm^{-1} [28, 29]. Due to cyanide nitrogen lone pair residing in a mostly $\text{C}\equiv\text{N}$ antibonding orbital, an increase of $\nu(\text{C}\equiv\text{N})$ in bridging cyanides ranges from 2150 to 2210 cm^{-1} for bridged tetracyanoplatinate(II) complexes [28]. The bridging cyanide frequencies in cyanide-bridged complexes are generally observed at higher frequencies, due to the kinematic coupling which is a mechanical constraint upon the bridging cyanide confined to the second metal [30]. The

Table 2. The wavenumbers of the $[\text{Pt}(\text{CN})_4]^{2-}$ vibrations in the complexes (cm^{-1}).

Assignments [27]	$\text{K}_2[\text{Pt}(\text{CN})_4]\cdot\text{H}_2\text{O}$	1	2	3
$A_{1g}, \nu(\text{C}\equiv\text{N})$	(2174) vs	(2192) vs	(2194) vs	(2192) vs
$B_{1g}, \nu(\text{C}\equiv\text{N})$	(2154) m	(2163) m	(2174) m	(2170) m
$E_u, \nu(\text{C}\equiv\text{N})$	2136 vs	2170 vs, 2146 vs	2158 vs	2149 vs
$E_u, \nu(\text{C}^{13}\text{N})$	2085 sh	2087 vw	2081 vw	2084 vw
$E_u, \nu(\text{M}-\text{C})$	504 m	504 m	502 w	504 vw
$A_{2u}, \pi(\text{M}-\text{CN})$	428 vw	419 vs	420 vs	428 vs
$A_{1g}, \nu(\text{M}-\text{C})$	(479) w	(469) w	(463) w	(461) vw
$E_u, \delta(\text{M}-\text{CN})$	407 s	408 sh	410 sh	412 s

Notes: s, strong, m, medium, w, weak, sh, shoulder, v, very. The symbols ν , δ and π refer to valence, in-plane and out-of-plane vibrations, respectively. Raman bands are given in parentheses.

$\nu(\text{CN})$ bands are observed as strong and sharp bands in the FT-IR and Raman spectra of the complexes. A splitting of the $\nu(\text{CN})$ mode is observed for **1**–**3**. Two strong bands are seen at 2170 cm^{-1} and 2146 cm^{-1} (**1**), but one strong band is observed in **2** and **3** [2158 cm^{-1} (**2**) and 2149 cm^{-1} (**3**)]. The two Raman fundamentals are assigned to 2192 and 2163 cm^{-1} (**1**), 2194 and 2174 cm^{-1} (**2**), and 2192 and 2170 cm^{-1} (**3**). These spectral data are in agreement with the structural data presented. According to this explanation, $\text{C1}\equiv\text{N1}$ and $\text{C2}\equiv\text{N2}$ bond lengths are $1.120(6)\text{ \AA}$ and $1.128(6)\text{ \AA}$ (**1**), $1.137(10)\text{ \AA}$ and $1.179(10)\text{ \AA}$ (**2**), and $1.130(4)\text{ \AA}$ and $1.136(4)\text{ \AA}$ (**3**). No splitting of CN stretching mode occurs in **2** and **3**, because bridging and terminal $\nu(\text{CN})$ absorption bands overlap. Similar situations have been observed in previous studies [5, 31]. In the low frequency region of the spectra, Pt–C stretches and Pt–CN bending bands from 504 to 419 cm^{-1} are observed for **1**, **2**, and **3**. In-plane bending vibration, $\delta(\text{M–CN})$ shifts to higher and lower frequencies. Such frequency shifts have been observed for the other ion pair charge transfer complexes [32].

3.2. Crystallographic analyses

Crystal data and structure refinement parameters for the complexes are presented in table 3. Selected bond lengths and angles are collected in table 4 and the hydrogen bonding geome-

Table 3. Experimental data for **1**, **2**, and **3**.

Complex	1	2	3
Empirical formula	$\text{C}_{18}\text{H}_{18}\text{N}_6\text{O}_2\text{PtCu}$	$\text{C}_{18}\text{H}_{18}\text{N}_6\text{O}_2\text{PtZn}$	$\text{C}_{18}\text{H}_{18}\text{N}_6\text{O}_2\text{PtCd}$
Color/shape	Green/block	Orange/block	Colorless/block
F_w	609.01	610.85	657.87
Temperature (K)	294	296	296
λ (Å)	Mo $\text{K}\alpha$ ($\lambda = 0.71073\text{ \AA}$)		
Crystal system	Triclinic	Triclinic	Monoclinic
Space group	$P-1$	$P-1$	$P2_1/n$
a (Å)	8.1553(3)	8.1938(2)	10.4344(4)
b (Å)	8.3859(3)	8.2462(2)	8.9240(3)
c (Å)	9.0503(4)	9.1324(3)	10.8621(4)
α (°)	117.001(4)	106.347(3)	90
β (°)	107.965(3)	115.776(4)	93.675 (3)
γ (°)	95.628(2)	98.954(2)	90
V (Å ³)	503.47(3)	504.84(4)	1009.36(6)
Z	1	1	2
μ (mm ⁻¹)	8.02	8.13	8.00
ρ (calcd) (Mg m ⁻³)	2.009	2.009	2.165
Max. crystal dimen. (mm)	$0.28 \times 0.23 \times 0.17$	$0.27 \times 0.24 \times 0.17$	$0.28 \times 0.21 \times 0.15$
Range of h	$-10 < h < 10$	$-10 < h < 10$	$-13 < h < 13$
Range of k	$-11 < k < 11$	$-11 < k < 11$	$-11 < k < 11$
Range of l	$-12 < l < 9$	$-11 < l < 12$	$-14 < l < 14$
No. of reflections total	8238	7793	16,711
No. of reflections unique	2520	2473	2521
No. of reflections with $I > 2\sigma(I)$	2458	2472	2086
Structure solution	direct methods		
R_{int}	0.054	0.049	0.062
$2\theta_{\text{max}}$ (°)	57.6	57	56.8
$T_{\text{min}}/T_{\text{max}}$	0.126/0.256	0.217/0.339	0.552/0.689
Number of parameters	134	134	135
Goodness-of-fit on F^2	1.08	1.08	1.09
R [$F^2 > 2\sigma(F^2)$]	0.026	0.039	0.027
R_w	0.067	0.105	0.082
$(\Delta\rho)_{\text{max}}$ (eÅ ⁻³)	1.48	2.36	1.60
$(\Delta\rho)_{\text{min}}$ (eÅ ⁻³)	-2.22	-4.43	-2.44

Table 4. Selected bond lengths (Å) and angles (°) for **1**, **2**, and **3**.

1		2		3	
<i>Bond lengths</i>					
Pt1–C1	1.995(4)	Pt1–C1	1.978(7)	Pt1–C1	1.978(3)
Pt1–C2	1.984(4)	Pt1–C2	1.958(6)	Pt1–C2	1.978(3)
Cu1–O1	2.347(3)	Zn1–O1	2.129(5)	O1–Cd1	2.293(3)
Cu1–N2	1.990(4)	Zn1–N2	2.125(6)	Cd1–N2	2.327(3)
Cu1–N3	2.049(3)	Zn1–N3	2.157(5)	Cd1–N3	2.316(2)
C1–N1	1.120(6)	C1–N1	1.137(10)	C1–N1	1.130(4)
C2–N2	1.128(6)	C2–N2	1.179(10)	C2–N2	1.136(4)
<i>Bond angles</i>					
C1 ⁱ –Pt1–C1	180.0(4)	C1 ⁱ –Pt1–C1	180.0(4)	C1–Pt1–C1 ⁱ	180.00(19)
C2–Pt1–C1	89.54(17)	C2–Pt1–C1	90.0(3)	C2–Pt1–C1	89.64(13)
C2 ⁱ –Pt1–C1	90.46(17)	C2 ⁱ –Pt1–C1	180.0(4)	C2 ⁱ –Pt1–C1	90.36(13)
C2–Pt1–C2 ⁱ	180.0(2)	O1–Zn1–O1 ⁱⁱ	180.000(1)	C2 ⁱ –Pt1–C1 ⁱ	89.64(13)
O1–Cu1–O1 ⁱⁱ	180.0	O1–Zn1–N3	92.9(2)	C2–Pt1–C2 ⁱ	180.00(5)
N2–Cu1–O1	87.83(17)	O1 ⁱⁱ –Zn1–N3	87.1(2)	O1 ⁱⁱ –Cd1–O1	180.0(2)
N2 ⁱⁱ –Cu1–O1	92.17(17)	N2–Zn1–O1	89.0(2)	O1–Cd1–N2	88.06(13)
N2 ⁱⁱ –Cu1–N2	180.0	N2–Zn1–O1 ⁱⁱ	91.0(2)	O1 ⁱⁱ –Cd1–N2	91.94(13)
N2–Cu1–N3	87.53(14)	N2 ⁱⁱ –Zn1–N2	180.000(1)	O1–Cd1–N3	84.28(10)
N2 ⁱⁱ –Cu1–N3	92.47(14)	N2–Zn1–N3	92.6(2)	O1 ⁱⁱ –Cd1–N3	95.72(10)
N3–Cu1–O1	86.16(13)	N2–Zn1–N3 ⁱⁱ	87.4(2)	N2–Cd1–N2 ⁱⁱ	180.0(2)
N3 ⁱⁱ –Cu1–O1	93.84(13)	N3–Zn1–N3 ⁱⁱ	180.000(1)	N3–Cd1–N2	85.45(10)
N3 ⁱⁱ –Cu1–N3	180.000(1)	Zn1–O1–H1	122(7)	N3 ⁱⁱ –Cd1–N2	94.55(10)
Cu1–O1–H1	119(9)	C9–O1–Zn1	125.7(4)	N3 ⁱⁱ –Cd1–N3	180.00(12)
C3–O1–Cu1	122.8(3)	C2–N2–Zn1	166.1(5)	Cd1–O1–H1	127(5)
C2–N2–Cu1	168.1(3)	C3–N3–Zn1	117.4(5)	C9–O1–Cd1	125.0(2)
C5–N3–Cu1	125.9(3)	C7–N3–Zn1	124.3(4)	C9–O1–H1	104(5)
C9–N3–Cu1	115.1(3)	N1–C1–Pt1	179.4(7)	C2–N2–Cd1	147.5(3)
N1–C1–Pt1	178.5(4)	N2–C2–Pt1	178.6(5)	C3–N3–Cd1	118.5(2)
N2–C2–Pt1	178.1(4)			C3–N3–C7	117.9(3)
				C7–N3–Cd1	123.1(2)
				N1–C1–Pt1	178.3(3)
				N2–C2–Pt1	178.2(3)

Note: Symmetry codes: [(i) $-x, -y, -z$; (ii) $-x+1, -y, -z+1$ (for **1**)], [(i) $-x, -y, -z$; (ii) $-x, -y-1, -z-1$ (for **2**)] and [(i) $-x+1, -y, -z$; (ii) $-x, -y, -z$ (for **3**)].

Table 5. Hydrogen-bond geometries (Å, °) for **1**, **2**, and **3**.

Complex	D–H···A	D–H	H···A	D···A	D–H···A
1	O1–H1···N1 ⁱⁱⁱ	0.87(7)	2.00(10)	2.732(8)	141(9)
2	O1–H1···N1 ⁱⁱⁱ	1.00(13)	1.69(15)	2.677(11)	173(16)
3	O1–H1···N1 ⁱⁱⁱ	0.79(6)	1.91(6)	2.686(5)	169(6)

Note: Symmetry codes: (iii) $x, y-1, z$ (for **1**); (iii) $-x+1, -y, -z$ (for **2**); (iii) $x-1/2, -y+1/2, z-1/2$ (for **3**).

tries are given in table 5. The molecular structures of the complexes, along with the atom-numbering schemes, are depicted in figure 3. The Pt ions are located on inversion centers and surrounded by four C≡N groups; the Pt–C and C≡N bond distances and C–Pt–C bond angles are [1.958(6)–1.995(4) Å], [1.120(6)–1.179(10) Å], and [89.54(17)–90.46(17)°], respectively. In all three compounds, the coordination around Pt ions is square-planar. The other metal (M) ions (M = Cu(II), Zn(II) and Cd(II) for **1**, **2**, and **3**, respectively) are also located on inversion centers and surrounded by N and O donors, the M–N and M–O bond distances and N–M–N and O–M–N bond angles are [1.990(4)–2.327(3) Å],

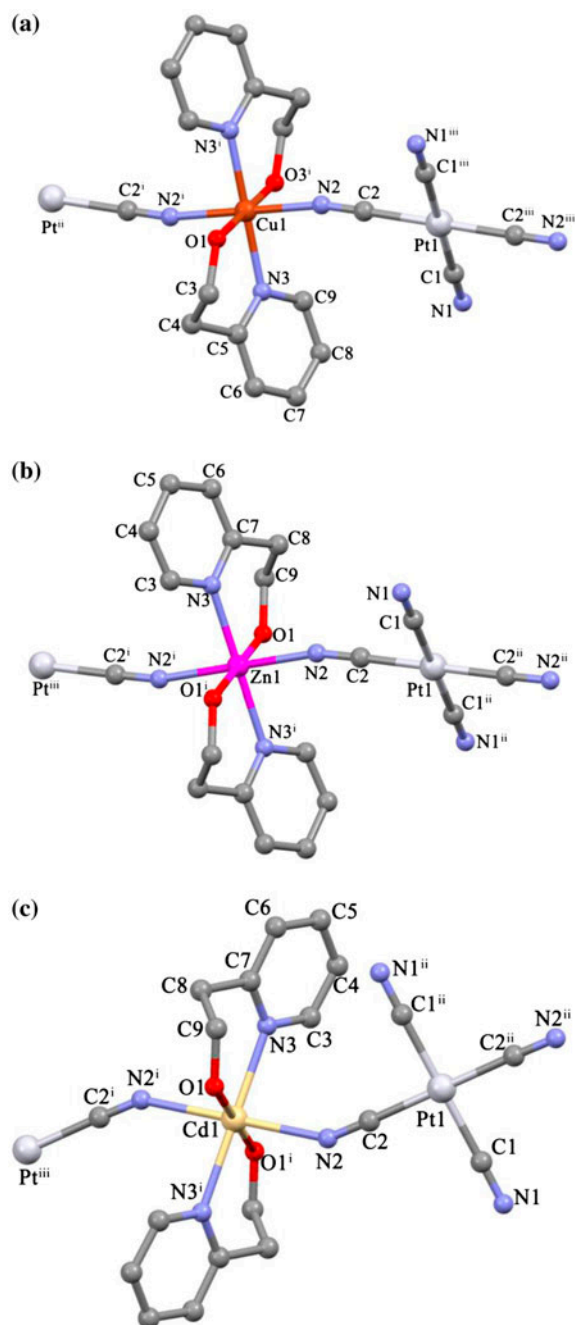


Figure 3. The molecular structures of **1** (a), **2** (b) and **3** (c) with the atom-numbering schemes. Symmetry codes: (i) $1-x, -y, 1-z$, (ii) $1+x, y, 1+z$, (iii) $-x, -y, -z$ (for **1**); (i) $-x, -1-y, -1-z$, (ii) $-x, -y, -z$, (iii) $x, -1+y, -1+z$ (for **2**); (i) $-x, -y, -z$, (ii) $1-x, -y, -z$, (iii) $-1+x, y, z$ (for **3**).

[2.347(3)–2.129(5) Å], [85.45(10)°–94.55(10)°], and [84.28(10)°–95.72(10)°], respectively. In all three compounds, the C≡N nitrogens and O of the ethanol groups in the equatorial plane around M form slightly distorted square-planar arrangements, while the slightly distorted octahedral coordinations are completed by the symmetric pyridine N donors in the axial positions.

The Cu(II) centers, which lie on crystallographic centers of symmetry, have distorted octahedral coordination; two nitrogens from hepH are located in the equatorial plane, and two symmetry-related nitrogens from cyanide occupy the axial positions. Due to the Jahn-Teller effect, the axial Cu1–O1 bond distance (2.347(3) Å) is longer than the equatorial ones with an average Cu–N value of 2.019 Å in **1** (table 4). These structural results are also supported by the spectroscopic analyses of the complexes. The N–Cu–N angles exhibit very similar values (N2–Cu1–O1 = 87.8(2)°); in [Cu(cyclam)Pt(CN)₄] a similar value of 86.20 (13)° was found [10]. These bond distances (Cu–N) are similar to the corresponding values (2.011(11) Å) in [Cu(cyclam)Pt(CN)₄] [10] and (2.0094(16) Å and 1.995(2) Å) in [Cu(mim)₂Pd(CN)₄]_n [33].

The most striking features of the complexes are the presence of the intermolecular C–H⋯Pt interactions between Pt and H of the hepH ligands: Pt1⋯H4A [2.8372(1) Å], Pt1⋯C4 [3.722(7) Å] and C4–H4A⋯Pt1 [152.0(4)°] (**1**), Pt1⋯H8B [2.7559(1) Å], Pt1⋯C8 [3.69(1) Å] and C8–H8B⋯Pt1 [163.0(6)°] (**2**), and Pt1⋯H8B [2.879(2) Å], Pt1⋯C8 [3.762(3) Å] and C8–H8B⋯Pt1 [152.0(2)°] (**3**). The C–H⋯Pt interaction for (R,R)–PtL complex was observed as H43B⋯Pt1B [2.910 Å], H6CA⋯Pt3B [2.988 Å], and H11A⋯Pt3B [3.066 Å] with the C–H⋯Pt angles of 145.6°, 145.5°, and 167.1° [34], distances of C22–H22B⋯Pt3 and C17–H17A⋯Pt4 interactions were found as 2.8043(2) Å, 2.9294(2) Å and the C–H⋯Pt angles were found as 172.1(3)° and 148.8(3)°, respectively, in [Cu₂(teta)₂Pt(CN)₄]₂[Pt(CN)₄]₂ [35].

Intramolecular O–H⋯N hydrogen bonds also exist between OH of hepH and N of cyanide. In the crystal structures, the intermolecular O–H⋯N hydrogen bonds link the polymeric chains into 2-D networks, effective in the stabilizations of the crystal structures (table 5 and figures 4, S1 and S2 [see online supplemental material at <http://dx.doi.org/10.1080/00958972.2015.1048239>]). The π⋯π contacts between the pyridine rings, Cg3–Cg3ⁱ [symmetry code: (i) 1 – x, 1 – y, 2 – z] (**1**), Cg3–Cg3ⁱ [symmetry code: (i) 1 – x, 1 – y, 2 – z] (**2**), and Cg3–Cg3ⁱ [symmetry code: (i) 1 – x, –y, 1 – z] (**3**), where Cg3 are the centroids of the pyridine rings, [(N3/C5–C9) (**1**), (N3/C3–C7) (**2**) and (N3/C3–C7) (**3**)], may further stabilize the crystal structures, with centroid–centroid distances of 3.934 Å (**1**), 3.969 Å (**2**), and 3.853 Å (**3**) (figures 4, S1 and S2). The X-ray structural determinations of all the complexes confirm the assignment of their structures from spectroscopic data.

3.3. Thermal analyses of the complexes

Thermal behaviors of the complexes are studied by TG, DTG, and DTA from 30 to 700 °C in dry air. The thermal analyses curves of the complexes are similar and the thermal decompositions of the complexes proceeded in two mass loss stages (figures 5 and S3). In the first stage, **1** started to lose one hepH between 198 and 330 °C (found 22.16%, calcd 20.22%). In the second stage of **1**, one hepH and four cyanide ligands (found 34.57%, calcd 37.30%) decomposed between 330 and 435 °C (DTA_{max} = 422 °C). The final solid products of the thermal decomposition were identified as CuO + Pt, calcd (found)% = 45.09% (42.48%). In the first stage, **2** and **3** started to lose two hepH ligands between 143 and 434 °C (found 40.95%, calcd 40.44%) for **2** and 162 and 419 °C (found 33.69%, calcd

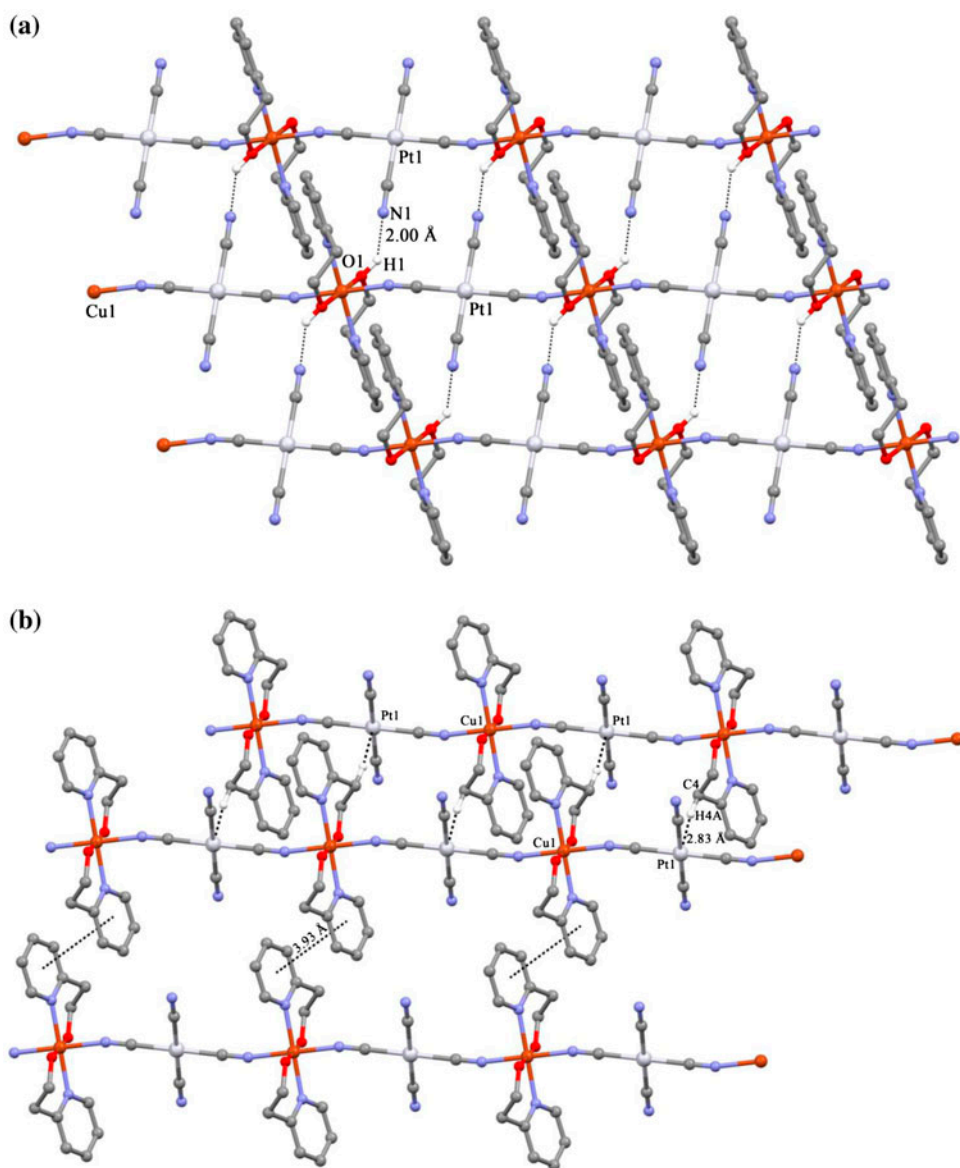


Figure 4. O-H...N interactions (a) and C-H...Pt and π ... π interactions (b) in 1.

37.43%) for **3**. In the second stage, four cyanides (found 14.80%, calcd 17.03%) decomposed between 434 and 496 °C ($\text{DTA}_{\text{max}} = 491$ °C) in **2** and 419 and 469 °C ($\text{DTA}_{\text{max}} = 465$ °C) for **3**. This peak was associated with decomposition and burning of the four cyanide ligands. The final solid products of the thermal decomposition were identified as ZnO + Pt, calcd (found)% = 45.26% (43.64%) for **2** and CdO + Pt, calcd (found)% = 49.14% (52.21%) for **3**. The thermal decomposition products were identified by FT-IR spectroscopy.

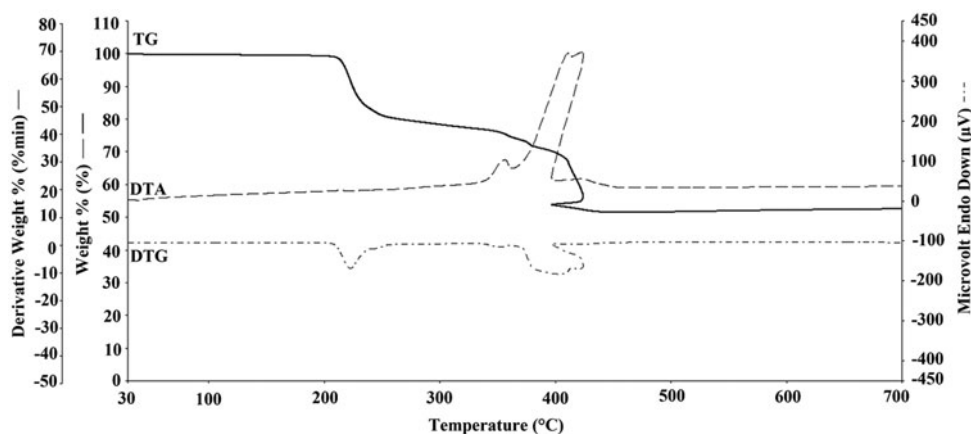


Figure 5. TG, DTG, and DTA curves of **1**.

4. Conclusion

Three heteronuclear cyanide complexes, $[\text{Cu}(\text{hepH})_2\text{Pt}(\mu\text{-CN})_2(\text{CN})_2]_n$ (**1**), $[\text{Zn}(\text{hepH})_2\text{Pt}(\mu\text{-CN})_2(\text{CN})_2]_n$ (**2**), and $[\text{Cd}(\text{hepH})_2\text{Pt}(\mu\text{-CN})_2(\text{CN})_2]_n$ (**3**), are prepared and investigated by spectroscopic, thermal, and diffraction techniques. The coordination environments of the M (II) ions (M = Cu(II), Zn(II), and Cd(II)) are described as distorted octahedral geometries, whereas the $[\text{Pt}(\text{CN})_4]^{2-}$ centers have square-planar geometries. The copper coordination sphere displays the usual axial deformation due to the Jahn-Teller effect. The structures of the complexes consist of 1-D linear chains in which the M(II) and Pt(II) ions are linked by cyanide bridges. As can be seen from the crystallographic data, the crystal packings of the complexes were composed of intermolecular C–H \cdots Pt interactions. In all of the complexes, $\pi\cdots\pi$ and O–H \cdots N interactions are observed. The presence of individual functional groups and the compositions of the complexes were proved by vibrational (FT-IR and Raman) spectroscopy and elemental analyses. The results from FT-IR and Raman spectral data were compared with the X-ray data. According to the spectral data, $\nu(\text{CN})$ stretching mode in the formation of cyanide bridge shifts higher frequencies. The study of thermal properties of the complexes showed two-step decomposition consisting of release of ligands and four cyanide groups from one formula unit.

Supplementary material

CCDC reference numbers 1032542 (for **1**), 1032543 (for **2**) and 1032541 (for **3**) contain the supplementary crystallographic data for this paper. These data can be obtained free of charge via <http://www.ccdc.cam.ac.uk/conts/retrieving.html> (or from the CCDC, 12 Union Road, Cambridge CB2 1EZ, UK; Fax: +44 1223 336033; E-mail: deposit@ccdc.cam.ac.uk).

Acknowledgement

This work was supported by the Research Fund of Eskişehir Osmangazi University (Project No. 201419A207). The authors are indebted to Anadolu University and the Medicinal Plants and Medicine Research Centre of Anadolu University, Eskişehir, Turkey, for the use of X-ray diffractometer.

Disclosure statement

No potential conflict of interest was reported by the authors.

References

- [1] A. Karadağ, İ. Önal, A. Şenocak, İ. Uçar, A. Bulut, O. Büyükgüngör. *Polyhedron*, **27**, 223 (2008).
- [2] S.L. James. *Chem. Soc. Rev.*, **32**, 276 (2003).
- [3] B.J. Holliday, C.A. Mirkin. *Angew. Chem. Int. Ed.*, **40**, 2022 (2001).
- [4] S.R. Batten, S.M. Neville, D.R. Turner. *Coordination Polymers: Design Analysis and Application*, Royal Society of Chemistry, London (2009).
- [5] A. Karadağ, A. Şenocak, İ. Önal, Y. Yerli, E. Şahin. *Inorg. Chim. Acta*, **362**, 2299 (2009).
- [6] K. Gör, G.S. Kürkçüoğlu, O.Z. Yeşilel, O. Büyükgüngör. *Inorg. Chim. Acta*, **414**, 15 (2014).
- [7] L.R. Falvello, M. Tomás. *Chem. Commun.*, **3**, 273 (1999).
- [8] L.R. Falvello, R. Garde, M. Tomás. *J. Cluster Sci.*, **11**, 125 (2000).
- [9] I. Escorihuela, L.R. Falvello, M. Tomás. *Inorg. Chem.*, **40**, 636 (2001).
- [10] J. Černák, J. Kuchár, M. Stolárová, M. Kajňaková, M. Vavra, I. Potočňák, L.R. Falvello, M. Tomás. *Transition Met. Chem.*, **35**, 737 (2010).
- [11] J. Atwood, W. Steed. *Supramolecular Chemistry*, Wiley, Chichester (2000).
- [12] R. Matsuda, R. Kitaura, S. Kitagawa, Y. Kubota, T.C. Kobayashi, S. Horike, M. Takata. *J. Am. Chem. Soc.*, **126**, 14063 (2004).
- [13] L. Brammer. *Dalton Trans.*, **16**, 3145 (2003).
- [14] C. Janiak. *J. Chem. Soc., Dalton Trans.*, 3885 (2000).
- [15] Y. Zhang, J.C. Lewis, R.G. Bergman, J.A. Ellman, E. Oldfield. *Organometallics*, **25**, 3515 (2006).
- [16] S.H. Crosby, R.J. Deeth, G.J. Clarkson, J.P. Rourke. *Dalton Trans.*, **40**, 1227 (2011).
- [17] H.W. Roesky, M. Andruh. *Coord. Chem. Rev.*, **236**, 91 (2003).
- [18] C. Janiak. *Dalton Trans.*, **16**, 2781 (2003).
- [19] G.S. Kürkçüoğlu, E. Sayın, K. Gör, T. Arslan, O. Büyükgüngör. *Vib. Spectrosc.*, **71**, 105 (2014).
- [20] E. Sayın, G.S. Kürkçüoğlu, O.Z. Yeşilel, T. Hökelek. *Spectrochim. Acta, Part A*, **132**, 803 (2014).
- [21] A. Bruker. Saint and SADABS, Bruker AXS Inc., Madison, WI (2005).
- [22] G. Sheldrick. *Acta Crystallogr., Sect. A*, **64**, 112 (2008).
- [23] D. Sajan, J. Binoy, B. Pradeep, K. Venkata Krishna, V. Kartha, I.H. Joe, V. Jayakumar. *Spectrochim. Acta, Part A*, **60**, 173 (2004).
- [24] K. Gör, G.S. Kürkçüoğlu, O.Z. Yeşilel, O. Büyükgüngör. *J. Mol. Struct.*, **1060**, 166 (2014).
- [25] D. Karaağaç, G.S. Kürkçüoğlu, O.Z. Yeşilel, T. Hökelek, H. Dal. *Z. Krist.*, **227**, 639 (2012).
- [26] D. Sweeny, I. Nakagawa, S.I. Mizushima, J. Quagliano. *J. Am. Chem. Soc.*, **78**, 889 (1956).
- [27] K. Nakamoto. *Infrared and Raman Spectra of Inorganic and Coordination Compounds. Part B., Applications in Coordination, Organometallic, and Bioinorganic Chemistry*, Wiley, New York (2009).
- [28] M. Vavra, I. Potočňák, M. Kajňaková, E. Čizmar, A. Feher. *Inorg. Chem. Commun.*, **12**, 396 (2009).
- [29] A.M. Golub, H. Köhler, V.V. Skopenko. *Chemistry of Pseudohalides*, Elsevier, Amsterdam (1986).
- [30] J. Ribas, A. Escuer, M. Monfort, R. Vicente, R. Cortés, L. Lezama, T. Rojo. *Coord. Chem. Rev.*, **193–195**, 1027 (1999).
- [31] J. Černák, J. Skoršepa, K. Abboud, M. Meisel, M. Orendáč, A. Orendáčová, A. Feher. *Inorg. Chim. Acta*, **326**, 3 (2001).
- [32] M. Zhou, K. Wang, Z. Men, S. Gao, Z. Li, C. Sun. *Spectrochim. Acta, Part A*, **97**, 526 (2012).
- [33] G.S. Kürkçüoğlu, K. Gör, O. Büyükgüngör. *Spectrochim. Acta, Part A*, **124**, 588 (2014).
- [34] X.-F. Shan, D.-H. Wang, C.-H. Tung, L.-Z. Wu. *Tetrahedron*, **64**, 5577 (2008).
- [35] M. Vavra, I. Potočňák, M. Dušek. *Inorg. Chim. Acta*, **409**, 441 (2014).